Global Navigation Satellite System (GNSS) Signal Monitoring Using a High-Gain Parabolic Dish System

Curtis Cohenour
Ohio University
cohenour@ohio.edu

Abstract

The author presents a high-gain dish antenna system for monitoring global positioning system (GPS) and other global navigation satellite system (GNSS) signals. The system includes a parabolic dish antenna, a rotator, and graphical user interface (GUI). The dish is lightweight with low wind loading and installed without a substantial support structure. The GUI controls operation of the antenna including calibration and tracking. The GUI is customizable and implemented in MATLAB. A calibration routine eliminates the need for precise angular installation of the mechanical components.

A five-parameter calibration model minimizes elevation and azimuth errors in tracking the satellites. The calibration provides a transformation from the rotator reference frame to the true geodetic reference frame. The calibration is automatically performed by acquiring and tracking satellites. The dish sweeps each tracked satellite in azimuth and elevation to determine the exact satellite location in the rotator frame. The satellite ephemeris identifies the geodetic location of the satellite. Computation of calibration parameters are computed using least squares, and minimizes the error between the transformed rotator coordinates and the true satellite position.

The system can record radio frequency (RF) data or receiver data. RF data allows the user to directly observe the GPS codes. The high gain and low noise provides receiver data with an extremely low carrier phase noise. In addition, multipath is near zero for the dish antenna. Receiver data can identify signal deformation, and satellite antenna gain and phase patterns. Results include an analysis of the tracking error and the impact of the error on the measurements.

The experimental results show that the antenna system can be quickly deployed and accurately aligned. Tracking errors of up to two degrees do not impact phase measurements. GPS multipath errors are minimal.

Introduction

The global positioning system (GPS) is a space-based system used for land and air navigation. A lesser-known but important use of GPS is timing for banking transactions and cellular communications. The GPS signal is spread spectrum and 30dB below the noise floor. The receiver operates by de-spreading the RF signal. Using a high gain antenna increases the

signal to noise ratio such that the spread spectrum "chips" can be observed. Investigating the details of the GPS signal requires low noise.

The goal of this work is to develop a lightweight semi-portable hi-gain antenna. Because the antenna is semi-portable, alignment by surveying is impractical. The antenna chosen is an aluminum frame covered with galvanized steel mesh; see Figure 1. This is lightweight and has a low wind loading. The rotator is commercially available. The positioning system is implemented as a MATLAB graphical user interface (GUI) and specifically designed to facilitate alignment with the satellite spatial reference frame.

The literature describes other high-gain systems for tracking global navigation satellite system (GNSS) satellite vehicles (SVs) (Wong, Phelts, Walter, & Enge, 2009; Gao, Chen, Lo, De Lorenzo, Walter, & Enge, 2008; Usman, Saleem, & Armitage, 2013; van Graas, Cohenour, Norris, Vinande, Gunawardena, & Carroll, 2015). In Wong et al. (2009), a 46m dish collects RF data. The data characterize signal deformation of GPS and wide area augmentation system (WAAS) satellites. A 1.8m dish (Gao et al., 2008) is used to investigate the interoperability of GPS and Compass-M1. A high-gain (13dBi) helical antenna is developed in Usman et al. (2013).

A solid 1.8 m dish (not shown) (van Graas et al., 2015) is used to investigate GPS signals. The rotator on the solid dish has a limited range in both azimuth and elevation. Mounting the dish on a trailer provides mobility. For example, positioning the dish under a forest canopy allows the investigation of multipath through foliage. A D-TA RF recorder collects data. In addition, van Grass et al. describe experiments using the subject of this paper, shown in Figure 1.

The system presented here has the advantages of being lightweight with low wind loading, inexpensive, and high performance. The dish system consists of the dish and rotator, the RF system, and the software system.

Figure 1. A high gain parabolic dish system for tracking GNSS satellites.

Figure 1 shows the dish installed at the Ohio University Airport located in Albany, OH. An "H" stand anchored to the ground with stakes and ratchet straps supports the antenna. The Ohio University experimental local area augmentation system (LAAS) facility houses the equipment. The LAAS shelter contains the rotator control, RF components, data collection, and control. Operation is currently done on site, but high speed Internet is available for remote operation in the future.

A mobile system like this or the 1.8m dish in van Grass et al. (2015) requires a means of calibration to align the antenna in earth centered earth fixed (ECEF). Portable devices such as a level and a compass can align the antenna to within a few degrees but not to the precision required for satellite tracking. A coordinate transformation and a method of calibration using the GPS satellites as truth is required to quickly align the antenna in ECEF coordinates.

A GPS receiver collects data for this paper. The data from the GPS receiver consist of code minus carrier (CMC) and carrier phase (CP) data. The data can define satellite antenna gain and group delay patterns.

Rotator System

The dish is an FPD1M9KIT mesh dish kit. It is 1.9m in diameter with a 6mm mesh reflecting surface, produced and sold by RF-Hamdesign in the Netherlands. The rotator is a Big RAS/HR Alpha-Spid from Alpha Radio in Edmonton, Alberta, Canada. The controller is an MD-01 from Alpha, with a PS-01 power supply. The controller has front panel buttons for moving the rotator, and programing. Communication of motion commands and rotator positions are by RS-232.

The dish is parabolic with an F/D ratio of 0.45. Three struts support the feed horn, as seen in Figure 1. The Antcom G8 LHCP antenna is attached to a plate at the end of the support struts. The plate spacing was originally designed for a dB Systems cross-vee dipole. The Antcom antenna is mounted on standoffs to provide the proper spacing between the dish and the antenna phase centers.

The SPID BIG-RAS/HR rotator can rotate 720° in azimuth, and 180° in elevation. The current software uses 360° degrees of azimuth and an elevation from 0° to 90°. This artificial azimuth restriction requires the recording of some SV passes in two segments. Improved cable management would allow for an expanded rang e of azimuth motion. Passes recorded with this modification would be in one segment.

Alignment and calibration are critical for accurate tracking of an SV. Alignment is the process of adjusting the rotator so that it is plumb and oriented in azimuth. Calibration is the process of tracking SVs and computing the necessary parameters to convert the measured azimuth and elevation of the rotator to ECEF coordinates. This section addresses alignment; calibration is discussed later.

Alignment consists of two steps, first zero azimuth is established by turning the rotator on the central support of the "H" stand. The rotator azimuth is set using a compass and compensating for magnetic declination. In this case, the rotator zero is true geodetic north. An accuracy of ±10 is possible. Next, the rotator is leveled using a machinist level in the north-south and east-west planes. The accuracy of this method is ±2°.

RF System

The RF system is shown in Figure 2. An Antcom Corp: Passive L1/L2 GPS (left hand circularly polarized (LHCP) antenna P/N: G7L1L2-L-P-XS-1 is used as a feed horn. This can be seen in Figure 1. This is a special order item with LHCP for use with a parabolic reflector. The Antcom G8 is a passive antenna, so a JCA Technology JCA12-4189T amplifier with a gain of 45dB is mounted at the feed horn. Twelve volt power for the JCA amplifier is provided via the feed line using a bias-tee located in the equipment shelter. RF power is supplied to a GWInstek GSP-730 spectrum analyzer via a mini-circuits ZAPD-2 power splitter (S1). Another splitter (S2) is used to provide RF to two NovAtel receivers, the monitor, and the data collect. Each of these receivers is fitted with a direct current (DC) block to eliminate receiver antenna power from the RF circuit.

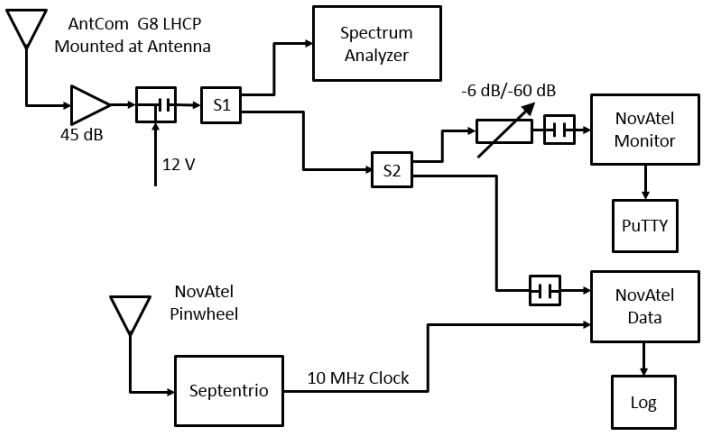

Figure 2. RF system.

The monitor receiver is used for calibration and monitoring. The receiver is a PWRPAK-4E-L1L2W version GPSCARD "L1L2W" "SPR02340052" "Euro4-1.02-222" "2.140" "1.002" "2004/Jan/20" "11:00:47." The signal-to-noise ratio at the output of splitter S2 is much higher than it would be using a non-directional antenna. The carrier to noise ratio (CNR) of the receiver is limited to 52 dB-Hz. To overcome this issue a variable RF attenuator is used to bring the CNR into the linear range of the NovAtel receiver. The receiver is programmed to output the American Standard Code for Information Interchange (ASCII) range log at 1Hz, "Log RangeA OnTime 1". The serial output is captured using the terminal program PuTTY, and written to a text file. The output file is read into MATLAB, and the ASCII range message is used for calibration and monitoring.

The data receiver has a custom software modification to provide GPS L1 accumulated Doppler range (ADR) at 100 Hz. The receiver is a PWRPAK-4E-L1L2W100 version GPSCARD "L1L2W100" "TPR00480113" "Euro4-1.00-222" "2.140S3" "1.002" "2003/Dec/11" "15:37:06." The binary log "Log Range OnTime .05" generates range data including pseudo range (PR) on L1 (PR1), PR on L2 (PR2), ADR on L1 (ADR1), and ADR on L2 (ADR2). The command "log GpsL1Adrb OnTime 0.01" generates the custom 100 Hz L1 ADR log. The output of the GpsL1Adrb log is processed using a NovAtel supplied utility *ProcessGPSL1ADR.exe*. This utility combines the GpsL1Adrb and the range logs into a custom 100Hz ADR1 measurement.

The monitor and data receivers track only one valid satellite and cannot generate a position and time solution. With no clock solution, the receiver operates in freewheeling clock mode with clock errors in the range of 100ms. This is not an issue for the monitor receiver, but the large constantly varying clock error interferes with the results of the data receiver. To resolve this issue a Septentrio NV PolaRxS^{PRO} receiver version vAB0201.AB0204.AA0101.100 is used as a clock source. The Septentrio receiver is connected to a NovAtel GPS-600 pinwheel antenna and generates a valid position and time solution. The Septentrio has a 10 MHz clock output and is connected to the clock input of the NovAtel data receiver. The commands "ExternalClock Rubidium 10MHz" and "ClockAdjust Disable" set up the NovAtel clock input and disable the clock adjust. The resulting NovAtel clock is then fixed with a constant error in the range of 100ms. Some slowly varying clock error from the Septentrio time solution remains in the clock signal but is removed later in data processing. This error is on the order of three meters or 10ns.

Software System

This section describes the software system used for monitoring the GPS signal, control of the dish, calibration, tracking, and other operations. These functions are tied to the dish controller and the monitor receiver. The data from the data receiver are covered in the next section. The software system can be operated in real time while connected to the rotator or in simulated mode. Simulated mode is used to test the software and can be operated faster than real time.

The dish control is implemented in a MATLAB GUI composed of several interactive windows. The main control window is shown in Figure 3 (left). This window includes buttons on the left for the primary functions of the control software with status lights on the right. The functions include starting and stopping the GUI, Sweep, Calibrate, Track, Scan, Scan and Sweep, Setup, and Stop. There is also a button for antenna pattern, but this function has not been implemented.

The functions Start GUI and Stop GUI start and stop the control. A red/green indicator to the right of the Start GUI button indicates that the GUI is running. The Stop GUI button also stops the motion of the rotator. The Sweep function sweeps the antenna ±6° in azimuth and ±6° in elevation. The Calibrate button runs the calibration routine with the intent of generating the parameters necessary to convert the raw azimuth and elevation from the

rotator to true azimuth and elevation. The Track button starts the tracking of an SV. The Scan button scans the constellation stopping for 10 seconds at each SV. The Scan and Sweep function scans the constellation but performs a sweep for each SV. This function is used to collect calibration data. The Setup button provides a means to set a variety of adjustable parameters. The Stop button stops the motion of the rotator.

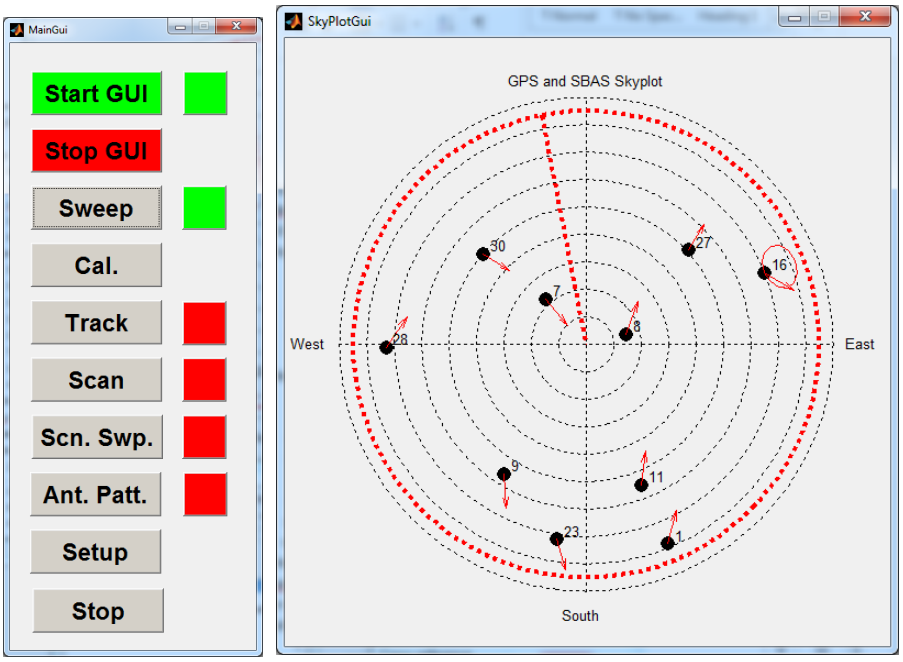

Figure 3. Main GUI control window (left), sky plot (right).

Figure 3 (right) shows an interactive Sky Plot GUI. The user may click on any location greater than the adjustable 5° elevation mask angle to move the rotator. The antenna location is shown as the red oval near SV pseudo random noise (PRN) 16. The antenna locator is a 6° circle in free space. It appears as an oval in Figure 3 (right) because the hemispherical sky distorts the planar projection. Clicking on an open area of the sky plot will cause the antenna to move to the selected position and clear the tracked SV. Clicking on or near an SV, indicated by a black dot and a number, will set the tracker to the SV and move the antenna to the desired SV. The direction and speed of each SV is indicated by a red arrow. Red dotted lines indicate the elevation mask and the location of the rotator zero azimuth. In the current version of the software the rotator will not cross the rotator zero azimuth. The rotator zero azimuth is indicated by the red dotted radial line at -10.9°.

The satellite positions and velocities are determined using the two-line elements (TLEs). The TLEs are downloaded from http://www.celestrak.com/NORAD/elements/ under Navigation Satellites/GPS Operational (CelesTrak, 2016). The GPS second of the week (SOW) is derived from the system time with the coordinated universal time offset. The function is called with the GPS SOW and returns the location and velocity of all the SVs above the mask in earth centered earth fixed coordinates. The position is converted to azimuth and elevation based on the user location (supplied by the user). The future position is computed adding

1000s to the SOW and calling the TLE function a second time. The future position is converted to azimuth and elevation. The SV positions are plotted and labeled. A red arrow is drawn from the SV position and its future positon to indicate the direction and velocity of the SV in azimuth and elevation.

The azimuth/elevation/CNR GUI display is tied to the monitor receiver and shown in Figure 4. There are plots of the azimuth vs. CNR and elevation vs. CNR. The L1 and L2 CNR and the tracked SV PRN are shown on the right. The button Set Az0 and the value of Az0 are located between the azimuth and elevation plots. The azimuth and elevation plots show the results of the sweep function. The read circle indicates the current measurement. The horizontal axis is the calibrated rotator azimuth less the SV azimuth. When the rotator sweeps, the CNR drops approximately with the square of the angular error between the antenna and the SV. Clicking on the azimuth graph stops all other rotator functions and moves the antenna to the indicated azimuth. For example, in Figure 4, clicking at +8° on the azimuth plot would move the antenna to +8°. If the SV were at 60°, then the rotator would move to a true azimuth of 68°. In this case, the Az0 is 349.1°, so the rotator azimuth would go to 78.9° because there is a difference of 10.9 degrees between the rotator zero and true north; see Figure 4.

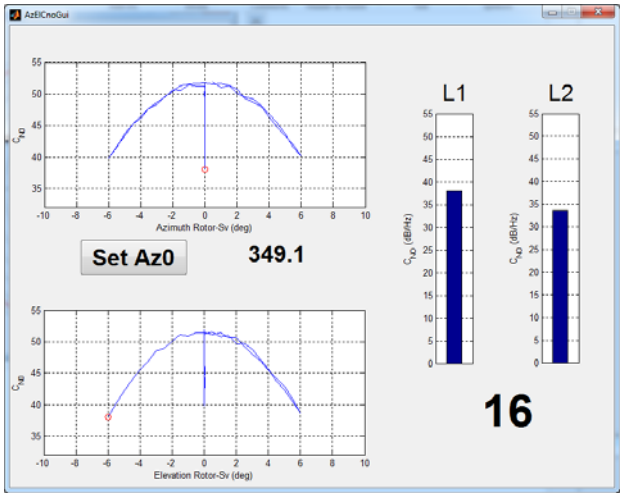

Figure 4. The interactive azimuth/elevation/CNR (AzElCNR) GUI window.

In addition to monitoring the azimuth/elevation/CNR, the GUI is used to set the rotator Az0. As mentioned above, if the rotator is carefully leveled the only unresolved error will be Az0. The SV CNR peak is found by adjusting the azimuth and elevation using the Azimuth /Elevation/CNR GUI, Figure 4. Once the peak is found, clicking the Set Az0 button sets Az0. With the Az0 set, the Scan and Track function can be used to collect calibration data. Additional GUIs (not shown) include manual control, setup, and debug information.

Calibration

Calibration defines the transformation from the rotator azimuth and elevation to true azimuth and elevation. The SVs are in the true coordinate system while the rotator coordinate system

is unknown. The calibration is performed by leveling the rotator and measuring the Az0 of the rotator. The rotator zero can be set to true north or any other convenient position. A rough calibration is performed by finding an SV and clicking the Set Az0 button as described above. The system is then placed in Scan and Sweep mode. This tracks the SVs one at a time and sweeps both azimuth and elevation. Data are automatically collected. Once all of the SVs have been scanned, the calibration is performed by pressing the Calibrate button, Figure 3 (left). Since some of the SV sweeps may not be centered, it is best to consider this a preliminary calibration. Once the preliminary calibration is completed, the GUI is restarted to clear the data collection. The scan and sweep can be run again for several passes and the calibration repeated. This time, the sweeps will generally be centered and provide accurate SV locations for the calibration. With practice, the total setup and calibration time is about two hours.

Figure 5 shows the azimuth and elevation for the calibration performed May 31, 2013. The blue lines indicate the rotator sweeps, while the red circles indicate the true SV position. The objective is to find model parameters that create the best fit.

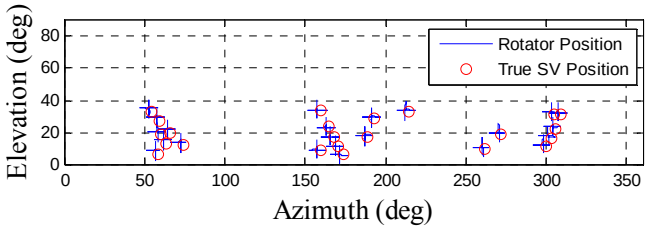

Figure 5. Azimuth and elevation for calibration data collected on May 31, 2016 with multiple sweeps for each SV, and the true SV location. The antenna travel between sweeps is not plotted.

For each SV observation, the first step is to determine the location of the peak in the CNR curve, as shown in Figure 6 (left). The blue dots show the elevation data collected. The red curve is a parabola fitted to the data. The peak is found for the rotator data and indicated by the large blue dot. The true SV position is plotted as a red dot. The data is plotted as the SV elevation less the rotator elevation. This compensates for the moving SV.

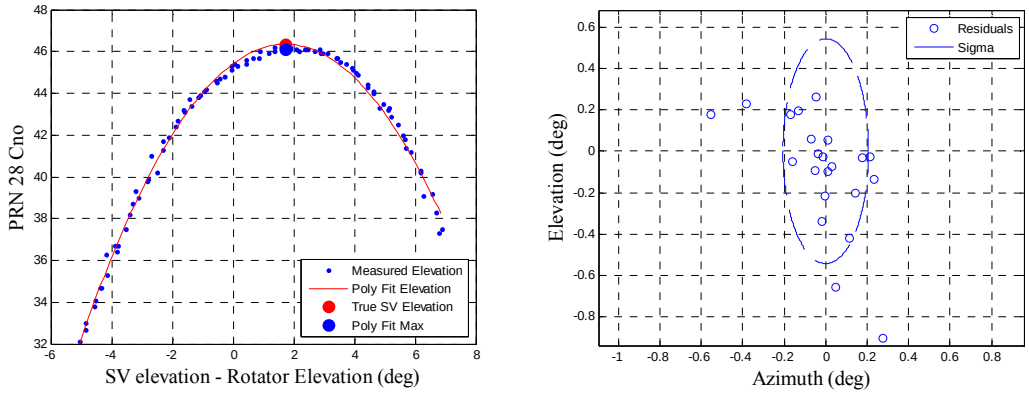

Figure 6. Identifying the peak in the CNR vs. elevation curve (left), residual errors(right).

The process above is repeated for each observation, which includes both elevation and azimuth. The results, in this example, are a set of 23 azimuth/elevation pairs in the rotator frame. In addition, there are 23 true azimuth/elevation pairs from the TLEs. Ordinary least squares (OLS) (Golub & van Loan, 1996) is used to find the best model parameters that fit the rotator data to the true SV position data. The results for the five parameter model are shown in Figure 6 (right): the circles show the errors for each observation; one outlier is not shown. The dotted oval is the standard deviation of the residuals including the outlier. The azimuth standard deviation is 0.2º while the elevation standard deviation is 0.5º.

The five parameter model is mathematically correct and uses direction cosine matrices to rotate the dish line of sight (LOS) to the true reference system. The antenna LOS may be offset from the moving end of the rotator. The rotator rotation is known. The alignment of the fixed end of the rotator in the true coordinate system is unknown. In the five parameter model, these values are computed and used to correctly point the antenna.

Table 1 lists the reference frames used in the five parameter model. The antenna LOS is $V^A = [1 \quad 0 \quad 0]^T$ where the superscript "T" indicates the transpose. V^A is in the antenna reference frame, the A-frame. There is likely some misalignment between the A-frame and the moving end of the rotator, which is defined as the B-frame. The rotator has azimuth and elevation angles that define the relationship of the moving end of the rotator with respect to the stationary end of the rotator. The B-frame is the moving end of the rotator and the R-frame is the stationary end of the rotator. The satellites are by definition in the navigation frame. There will be misalignment between the stationary end of the rotator (R-frame) and the navigation frame or N-frame. See Table 1 for a summary of the reference frames.

Table 1. Reference frames for the five parameter calibration.

Reference System	Symbol
Antenna	A

Rotator Body (Moving End)	B
Rotator (Stationary End)	R
Navigation	N

Converting the antenna LOS from the A-frame to the N-frame requires a series of coordinate frame rotations. The rotation matrix is defined in the navigation literature (Titterton & Weston, 2004) for the conversion from the aircraft body to the navigation coordinate system as

$$C_N^B = f_R(\Theta) \quad (1)$$

Where Θ is a column vector of the three rotational angles, roll, pitch, and yaw

$f_R(\Theta) = \begin{bmatrix} \phi \\ \theta \\ \psi \end{bmatrix} = \begin{bmatrix} roll \\ pitch \\ \psi\ yaw \end{bmatrix}$ is defined in Titteton & Weston (2004).

C_N^B is a 3×3 transformation matrix

Table 2 summarizes the rotational parameters. The antenna LOS is a unit vector in X^A direction. The rotation wrt to the moving end of the rotator is given by Θ^B. The two components of Θ^B are calibrated parameters. The rotation of LOS vector in the B-frame to the R-frame is given by Θ^R. Θ^R contains the elevation and azimuth angles of the rotator. The misalignment of the rotator with respect to the navigation frame is contained in Θ^N. Examination of the source column in Table 2 shows five calibrated parameters: $\theta^B, \psi^B, \phi^N, \theta^N, \psi^N$. The azimuth and elevation of the rotator, parameters θ^R and ψ^R, are known.

Table 2. Rotational parameters for the five parameter calibration model.

Rotation	Source	Symbol	Description
$\Theta^B = \begin{bmatrix} 0 \\ \theta^B \\ \psi^B \end{bmatrix}$	Calibration	θ^B	Elevation of Antenna LOS with the moving end of the rotator
	Calibration	ψ^B	Azimuth (Left / Right) with the moving end of the rotator
$\Theta^R = \begin{bmatrix} 0 \\ \theta^R \\ \psi^R \end{bmatrix}$	Rotator	θ^R	Rotator Elevation
	Rotator	ψ^R	Rotator Azimuth
Θ^N	Calibration	ϕ^N	Roll of the fixed end of the rotator with the True Reference Frame

$= \begin{bmatrix} \phi^N \\ \theta^N \\ \psi^N \end{bmatrix}$	Calibration	θ^N	Roll of the fixed end of the rotator with the True Reference Frame
	Calibration	ψ^N	Roll of the fixed end of the rotator with the True Reference Frame

The following equation converts the antenna LOS vector in the A-frame to a vector in the N-frame as defined in Table 1 using the parameters from Table 2.

$$\mathrm{V}^N = C_R^N C_B^R C_A^B V^A \quad (2)$$

Where $V^A = \begin{bmatrix} 1 \\ 0 \\ 0 \end{bmatrix}$ $C_A^B = \mathrm{f_R}\begin{pmatrix} 0 \\ \theta^B \\ \psi^B \end{pmatrix}$ $C_B^R = \mathrm{f_R}\begin{pmatrix} 0 \\ \theta^R \\ \psi^R \end{pmatrix}$ $C_R^N = \mathrm{f_R}\begin{pmatrix} \phi^N \\ \theta^N \\ \psi^N \end{pmatrix}$

Data Processing

In this paper, there are three primary goals of the data processing: to examine the multipath errors, to measure the phase noise, and to investigate how dish misalignment impacts the measurements. Range data are collected at 20 Hz, and ADR1 data are collected at 100 Hz, as described above. An external clock is used to limit clock errors in the data collection receiver.

Data processing for all files proceeds as follows: first, the binary range data is parsed extracting 20Hz for the, PR1, PR2, ADR1, ADR2, PRN, and GPS SOW. Next, data from the 100Hz GpsL1Adr log is extracted, consisting of ADR1, SOW, and PRN. The data are trimmed to remove transients during acquisition and loss of signal. There are two time bases involved, 20Hz and 100Hz, and two ADR1 measurements.

The ionosphere delay free (IF) CMC (Kaplan, 1996) is computed for the 20 Hz data and shown in Figure 7 (right). The SV passes through 0° rotator azimuth requiring the rotator to reposition. Figure 7 (right) shows a small gap of 5.2 minutes in the data at hour 21.7. The carrier phase ambiguity changed when the SV was reacquired. The change in carrier phase ambiguity is removed from the data in Figure 7. There is an approximate 0.6m dip in the CMC due to tropospheric delay, which varies with SV elevation (Figure 7, left).

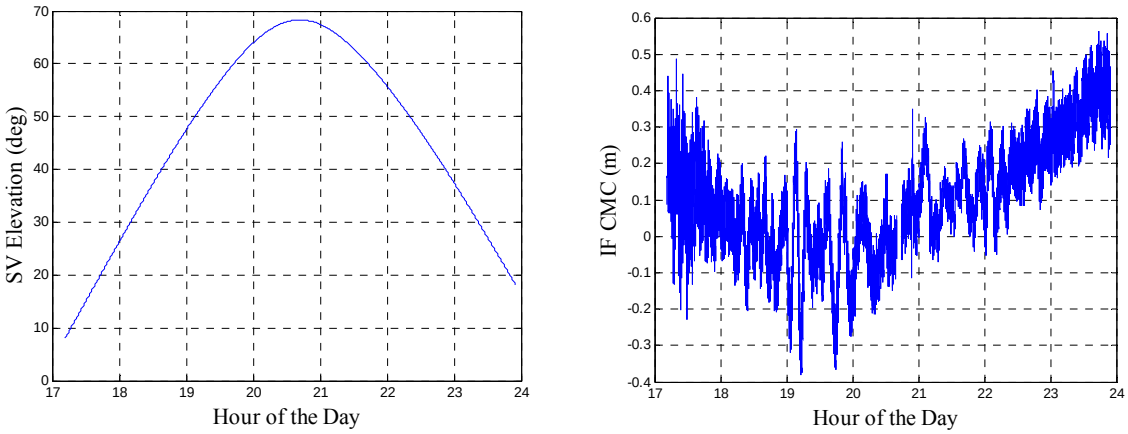

Figure 7. SV elevation (left), 20Hz IF CMC (right) for SV17 using data collected on June 24, 2016.

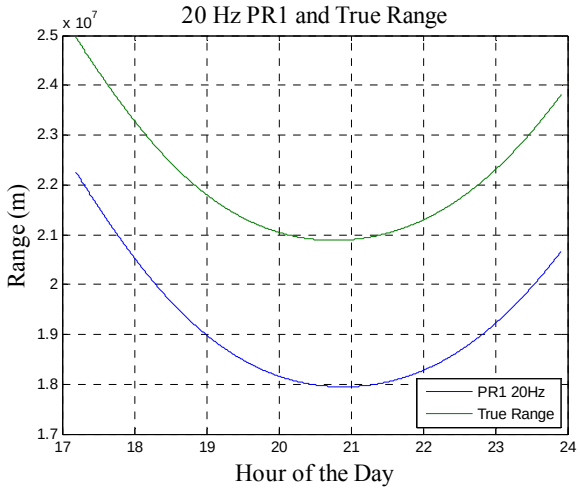

Figure 8. True range and PR1 data for SV17 on June 24, 2016.

The true location of the SV is extracted from the National Geospatial-Intelligence Agency (NGA) Antenna Phase Center files in SP3 format (Hilla, 2010; National Geospatial, FTP, 2016). The SP3 data contain the satellite position and the satellite clock at 15-minute intervals. The clock values are synchronized with GPS time. Overall accuracy of the NGA orbit data is given with respect to International GNSS Service (IGS) orbit data and is 7.1cm 3D RMS for orbit data ((National Geospatial, GPS, 2016). The true SV position and clock are interpolated onto the time scales using the MATLAB interp1 function and the "spline" option. The true range is computed by subtracting the origin in ECEF from the true SV position and taking the norm. The true range is offset by the SP3 clock adjust such that it matches the pseudo-range.

Figure 8 plots range data for SV17 on June 24, 2016. Note there is a large offset between the two curves. This is due to the large clock offset in the data receiver. The range offset is 2,925,000m or 9.8ms. The data receiver has a stabilized clock input, but there is no mechanism for the receiver to compute a time solution. This is corrected by removing a 10th order polynomial,
Figure 9 (left), from the data.

Removing a 10th order polynomial from the 100 Hz ADR1 yields a corrected ADR1 (ADR1C). The 100 Hz ADR1C data is plotted in Figure 9 (right). The remaining errors are attributable to the clock solution error in the Septentrio receiver.

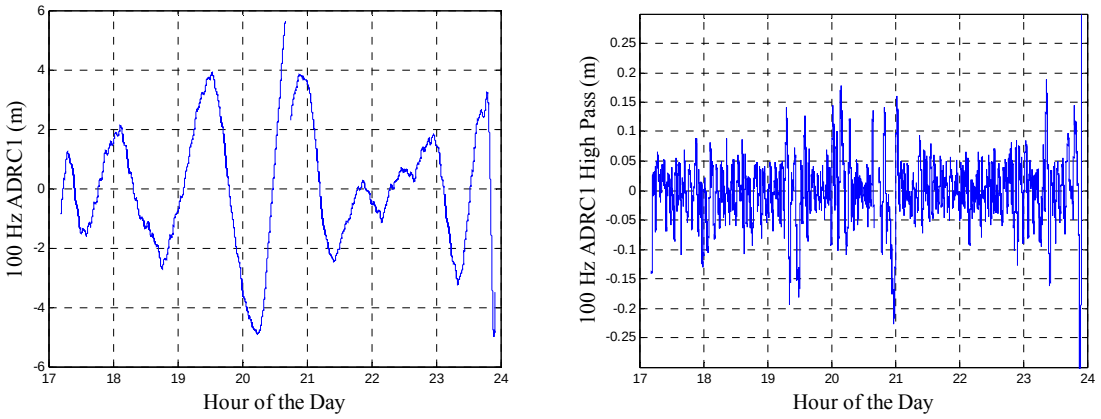

Figure 9. 100Hz ADR1C with four pole Butterworth high pass filter (left), after removal of polynomial curve fit (right), for SV17 on June 24, 2016.

The phase noise is calculated by taking the time difference of the 100 Hz ADR1C from Figure 9 (right).

$$\Delta\text{ADR1C} = \text{ADR1C}_{t_{k+1}} - \text{ADR1C}_{t_k} \qquad (3)$$

Where t_{k+1} and t_k are consecutive samples of ADR1C.

The result is shown in Figure (left). The probability density function (PDF) is shown in Figure (right).

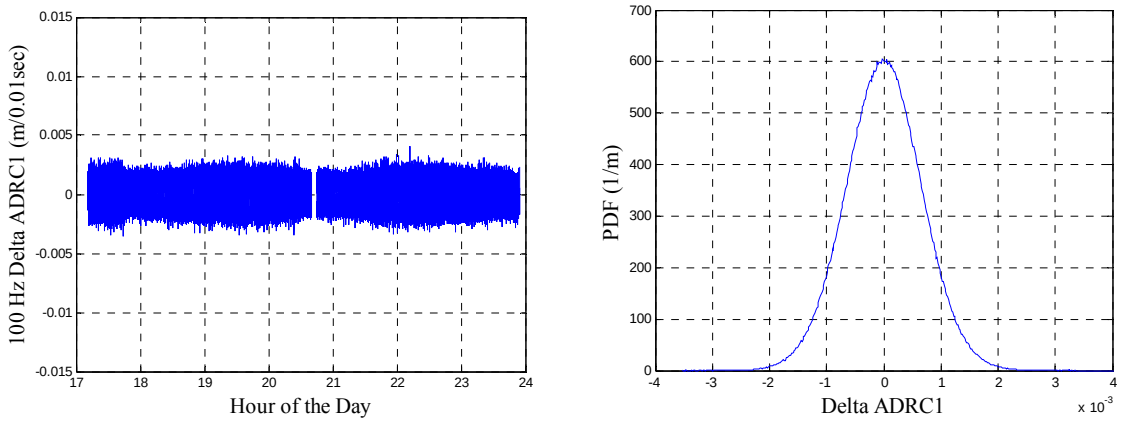

Figure 10. Delta ADR1C phase noise (left), and the PDF (right), for SV17 on June 24, 2016.

One final question is, will the dish pointing accuracy impact the results? Pointing errors are caused by calibration errors, positioning errors, and TLE errors. To answer this question, a dither signal was introduced to purposely offset the antenna, and the results examined. Using the five parameter model, the standard deviation of the residuals is 0.162° for azimuth and 0.176° for elevation. Thus, we might expect azimuth and elevation errors of 0.5°. The positioning dead band is 0.1° based on data collected while tracking an SV. The TLE errors are similar to almanac errors (Kelso, 2007) and on the order of 10 km. The range to the SV is 20 to 25 million meters; dividing by 10km and using the small angle approximation for the sine, the error is 0.03°. The time is verified using the debug display and accurate to within one second. The SV moves about 4,000 m/sec, which results in a time sync error of 0.01°. Thus, the TLE error is essentially zero compared to the other errors. The total tracking error is less than 1º.

To determine the impact of antenna misalignment, a temporary modification was made to the rotator GUI to insert dither into the dish pointing system. As the SV is tracked, a dither signal of ±2° max is placed on the azimuth and elevation of the dish as shown in Figure 10. The dither signal in Figure 10 is scaled for presentation. Each step of the dither signal is 5s long. The dither is keyed to GPS time to facilitate time registration with the data during processing.

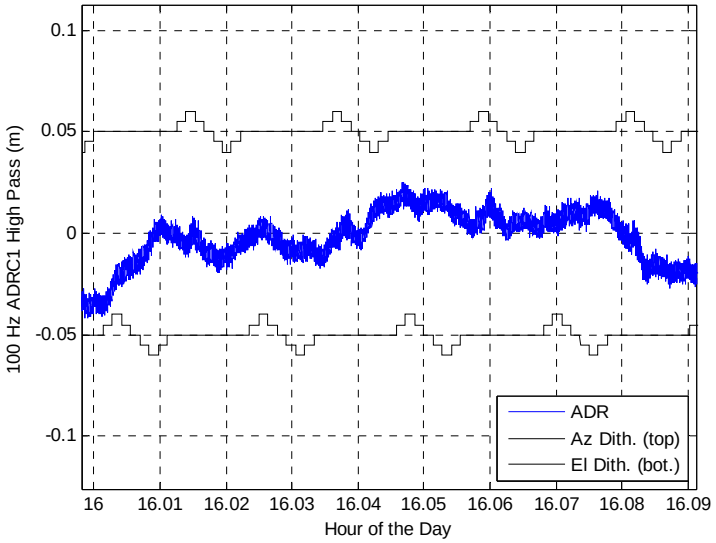

Figure 10. Data collected to determine the impact of antenna misalignment. Dither signals are ±2° maximum. The dither is keyed to GPS SOW to eliminate issues in time registration of the dither and the data. The magnitude of the dither signal is not to scale.

OLS (Gao et al., 2008) was used to fit the dither to the data using the equation,

$$\widetilde{\emptyset_1^c} = \emptyset_1^c - \propto_1 D_{Az} - \propto_2 D_{El} \qquad (4)$$

Where $\emptyset_1^c$ is the 100 Hz corrected ADR, ADR1C
D_{Az} is the azimuth dither degrees
D_{El} is the elevation dither in degrees
$\propto_1$ and $\propto_2$ are unknowns in the OLS solution and have units of m/deg
$\widetilde{\emptyset_1^c}$ is the modeled $\emptyset_1^c$ with dither impacts removed

We want to find $\propto_1$ and $\propto_2$ to minimize $\widetilde{\emptyset_1^c}$, that is $\widetilde{\emptyset_1^c} = 0$.

The results of the misalignment or dither test are given in Table 3. With $\propto_1$ and $\propto_2$ set to zero, the $\widetilde{\emptyset_1^c}$ is the same as ADR1C, and the standard deviation is 0.027 526 189m. With $\propto_1$ and $\propto_2$ set to the values in Table 3, minimizing the dither corrected ADR1C, $\widetilde{\emptyset_1^c}$; the standard deviation is 0.027 516 169m. The difference is .020µm. The conclusion is that dish misalignment of ±2° has no impact on ADR1C.

Table 3. OLS solution results for the misalignment (dither) test.

Case	Az. Multiplier m/deg $\propto_1$	El. Multiplier m/deg $\propto_2$	Standard Deviation
No Comp.	0	0	0.027 526 189
OLS values	0.000 641	0.000 400	0.027 516 169

Conclusion

The performance of the lightweight dish and associated RF and control components have been evaluated. Performance in multipath, phase noise, pointing accuracy, calibration have been investigated. Multipath performance for the system is ±30cm for IF CMC and ±20cm for L1 ADR. Phase noise is ±3mm for L1 at 100 Hz.

An improved calibration model was developed and tested. The model accurately accounts for errors in the antenna LOS with respect to the rotator and alignment of the rotator in the navigation coordinates. Results of the calibration are an azimuth residual standard deviation 0.2º while the elevation residual is standard deviation is 0.5º.

The pointing accuracy of the dish is ±1°. An evaluation of the dish performance shows there is no L1 ADR error for dish pointing errors of up to ±2°.

Data for several SVs were collected. All of the SVs are Block Type IIR or IIR-M running on rubidium clocks. The phase noise is ±.4cm for all SVs except PRNS 28 and 21. PRN 28 is ±0.6cm. PRN 21 is known to have phase noise spikes. The underlying phase noise is ±.4cm, while the spikes are ±1.5cm.

The research presented here was completed in August 2015. Since that time, the system has been used to study phase anomalies in the GPS Satellite Vehicle Number 63, which broadcast as pseudo random noise code 1 (see Ramesh, Ugazio, & van Graas, 2007). The solid dish (see van Graas et al., 2015) using the same software with an alternate rotator will be used for pulsar measurements. Finally, the software is being applied to an alternate antennas system to perform low-frequency WWVB measurements on CubeSats (n.d.).

The system presented here is easily deployable and can be used with an RF data recorder or a GPS receiver. Because a mobile or semi-mobile system is difficult to mechanically align in ECEF coordinates, a calibration means is provided. The calibration method is quick and accurate. The system provides low noise GPS data for analysis of signal deformation, satellite antenna gain and phase measurement, multipath investigations.

References

CelesTrak. (2018). Retrieved from http://www.celestrak.com/NORAD/elements/

CubeSat. (n.d.). *Origin of the new space revolution*. Retrieved from http://www.cubesat.org/

Gao, G., Chen, A., Lo, S., De Lorenzo, D., Walter, T., & Enge, P. (2008). Compass-M1 broadcast codes and their application to acquisition and tracking. *Proceedings of Institute of Navigation National Technical Meeting*. Manassas, VA: Institute of Navigation.

Golub, G., & van Loan, C. (1996). *Matrix computations*. (3rd ed.). Baltimore: The John Hopkins University.

Hilla, S. (2010). *The extended standard product 3 orbit format (SP3-c)*. Silver Springs, MD: National Geodetic Survey.

Kaplan, E. D. (1996). *Understanding GPS: Principles and applications*. Boston: Artech House Publishers.

Kelso, T. S. (2007). Validation of SGP4 and IS-GPS-200D against GPS precision ephemeris. *Proceedings of the 17th AAS/AIAA Space Flight Mechanics Conference*. Springfield, VA: AAS.

National Geospatial Intelligence Agency. (2016). *NGA/IGS GPS orbit (ephemeris) comparison page*. Retrieved from http://earth-info.nga.mil/GandG/sathtml/ngaigscompare.html

National Geospatial Intelligence Agency. (2016). *NGA FTP directory*. Retrieved from ftp://ftp.nga.mil/pub2/gps/apcpe/2016apc/

Navigation Center. (n.d.). *GPS constellation status for 08/02/2016*. Retrieved from http://www.navcen.uscg.gov/?Do=constellationstatus

Ramesh, R., Ugazio, S., & van Graas, F. (2017). Characterization of GPS satellite phase anomalies for SVN 63 (PRN 1) using a dish antenna. *Proceedings of the ION 2017 Pacific PNT Meeting*. Manassas, VA: Institute of Navigation.

Titterton, D. H., & Weston, J. L. (2004). *Strapdown inertial navigation technology*. (2nd ed.) Reston, VA: The American Institute of Aeronautics and Astronautics.

Usman, M., Saleem T., & Armitage, A. D. (2013). Design, assembly and testing of a high gain LHCP helical antenna for reception of reflected GPS signals. *Progress In Electromagnetics Research, 44*, 161-174.

van Graas, F., Cohenour, C., Norris, N., Vinande, E., Gunawardena, S., & Carroll, M. (2015). GNSS signal characterization and monitoring using high gain antennas. *Proceedings of the 28th International Technical Meeting of The Satellite Division of the Institute of Navigation*. Manassas, VA: Institute of Navigation.

Wong, G., Phelts, E., Walter, T., & Enge, P. (2009). Characterization of signal deformations for GPS and WAAS satellites. *Proceedings of the 22nd International Technical Meeting of the Satellite Division of the Institute of Navigation*. Manassas, VA: Institute of Navigation.

Biography

Dr. Cohenour is an assistant professor in the Ohio University Engineering Technology and Management Department, in Athens, Ohio. He received a Bachelor of Science degree from West Virginia Institute of Technology in 1980, a Master of Science degree from Ohio University in 1988, and a PhD in Electrical Engineering from Ohio University in 2009. He is a registered professional engineer in West Virginia and Ohio.

Dr. Cohenour has worked in industry as an electrical engineer in the areas of control systems, automation, and power. He joined Ohio University in 2002 as a research engineer working for the Ohio University Avionics Engineering Center. He has worked on projects covering a wide variety of avionics and navigation systems such as, the instrument landing system, microwave landing system, distance measuring equipment, LAAS, WAAS, and GPS.

His recent work has included research with the Air Force Research Laboratory in Dayton, Ohio, aimed at understanding and correcting image geo-registration errors from a number of airborne platforms. Contact Dr. Cohenour at cohenour@ohio.edu.